Journal of Energy Storage 75 (2024) 109715

Contents lists available at ScienceDirect

Journal of Energy Storage

journal homepage: www.elsevier.com/locate/est

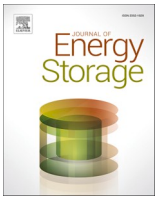

Research papers

Thermal stability and durability of solar salt-based nanofluids in concentrated solar power thermal energy storage: An approach from the effect of diverse metal alloys corrosion

Adela Svobodova-Sedlackova [a], Anabel Palacios [b], Zhu Jiang [b], A. Ines Fernández Renna [a], Yulong Ding [b], Helena Navarro [b], Camila Barreneche [a,*]

[a] Department of Material Science and Physical Chemistry, Universitat de Barcelona, c/Martí i Franqués, 1-11.08028, Barcelona, Spain
[b] Birmingham Centre for Energy Storage, School of Chemical Engineering, University of Birmingham, Birmingham B15 2TT, UK

ARTICLE INFO

Keywords:
Nanofluids
Corrosion test
Thermal energy storage (TES)
Chemical composition
Concentrated solar power plants (CSP)

ABSTRACT

Concentrated Solar Power (CSP) technology has witnessed substantial growth, with forecasts predicting an increase of 3.4 GW between 2019 and 2024. This expansion necessitates the installation of energy storage systems to meet the growing demand. Solar molten salts, specifically a mixture of 60 % $NaNO_3$ and 40 % KNO_3, have emerged as the primary thermal energy storage (TES) medium in commercial CSP plants. However, a significant challenge lies in the corrosive nature of molten salt at high temperatures, which poses limitations in TES applications. The literature has explored a promising solution: reducing corrosion rates by incorporating nanoparticles into molten salts, creating nanofluids. To assess the viability of nanofluids for CSP, it is essential to understand how they perform under working conditions, especially regarding their thermal stability and durability. This study presents further evidence of nanofluid interactions with component materials under static working conditions. Specifically, focus on the impact of corrosion products precipitated during corrosion tests on the physical and thermal properties of Solar Salt-based silica dioxide nanofluids. In this research, nanofluids in contact with stainless steel, nickel-chromium alloy, and carbon steel were examined before and after subjecting them to a 90-day thermal exposure at 500 °C. These findings provide valuable data on key thermo-physical properties during service, contributing to the design of more precise TES systems and enhancing their overall efficiency and effectiveness.

1. Introduction

Solar energy technologies hold significant potential for growth, primarily due to the abundant energy available during daylight hours for clean electricity generation using various technologies, such as solar power. Among these technologies, Concentrated Solar Power (CSP) plants stand out as they utilize mirrors to concentrate sunlight onto receivers, enabling the production of electricity. CSP is currently the most widely adopted solar energy technology on a large gigawatt (GW) scale. The sector is projected to experience substantial growth, with an anticipated increase of 3.4 GW between 2019 and 2024 [1]. CSP typically integrates thermal energy storage systems, allowing electricity generation during overcast periods and the storage of excess energy. Consequently, the combination of CSP and Thermal Energy Storage (TES) holds promise for delivering firm capacity - that is, generating electricity consistently and reliably during peak demand hours [2]. The inclusion of TES systems provides dependable energy dispatchability, ensuring a continuous electricity generation process. To achieve this, CSP plants require backup systems [3]. Moreover, TES systems enhance energy efficiency, defined as the ratio between useful output and input in an energy conversion process, thereby achieving the same task with less energy input. This improvement contributes to cost-effectiveness and optimized capital investments. Despite these advantages, the cost per kilowatt-hour of thermal energy ($/kWh$_{th}$) (total cost of TES divided by the storage capacity) remains a significant hurdle for CSP to compete with conventional energy sources and gain a substantial share in the energy market [4]. Various technologies can implement TES in conjunction with CSP, with the two-tank system emerging as the most prevalent TES configuration in recent years [5,6]. In this system, a heat transfer fluid (HTF) circulates between two tanks, facilitating the

* Corresponding author.
E-mail address: c.barreneche@ub.edu (C. Barreneche).

https://doi.org/10.1016/j.est.2023.109715
Received 20 July 2023; Received in revised form 7 November 2023; Accepted 11 November 2023

transfer of heat to the TES system through heat exchangers, for charging or discharging heat to the steam generator. One of the tanks maintains a low temperature (cold tank, ~288 °C) and is heated by the solar field, while the other tank stores heat at high temperatures (hot tank, ~388 °C).

Currently, molten salts, specifically the eutectic mixture of 60:40 $NaNO_3$-KNO_3, so-called solar salts, stand as the predominant choice for TES in CSP plants [7,8]. Solar salts offers notable advantages, characterized by its thermal stability and cost-effectiveness [9]. However, the adoption of solar salts as TES materials introduces its set of challenges, including corrosion concerns and suboptimal thermal properties. Corrosion stands out as a primary apprehension within this system, emphasizing the crucial need for durable and reliable materials in high-temperature molten salt CSP applications. This issue can be mitigated by employing high-performance component materials for storage tanks, heat exchangers, pipes, and receivers, as suggested by the literature [10,11]. Nevertheless, this approach inevitably escalates the overall investment costs associated with CSP. It's important to recognize that the initial investment costs significantly contribute to the ultimate price of the electricity generated [12].

Addressing the second challenge previously mentioned, the issue of poor thermal properties has been tackled through the incorporation of highly thermally conductive particles ranging from micro to nanoscale [13]. In recent years, nanofluids have emerged as an enticing option for TES systems [14–16]. Nanofluids involve introducing a low concentration of nanoparticles (<5 % wt.) into molten salt, creating a colloidal system with suspended nanoparticles [17]. The most compelling feature of nanofluids, making them an attractive TES alternative, is their significantly improved thermophysical properties, including specific heat capacity (c_p) and thermal conductivity (κ). Molten salt-based nanofluids have exhibited enhancements of up to 30 % in c_p [18,19] and up to 70 % in κ [10,20,21].

Despite these promising advantages and potential applications of nanofluids, their practical utilization remains constrained by various uncertainties. These include their performance under operational conditions, susceptibility to chemical corrosion, susceptibility to mechanical erosion/abrasion, and possible interactions with components of the circuits and equipment involved [22]. Notably, the high corrosion observed when using molten salts at elevated temperatures remains a primary drawback and limitation in TES applications. A decreasing trend in corrosion rates with the incorporation of nanoparticles into molten salts is indicated by existing literature [23–27], suggesting that an oxide layer is formed at the steel-salt interface, which acts as a protective passive layer. However, it is essential to consider the corrosive impact of the tank on the liquid medium. Tank material corrosion can lead to the release of particles into the liquid medium, resulting in variations in chemical composition, altering liquid behaviour, and affecting physicochemical properties. Therefore, a comprehensive study of the behaviour of physicochemical properties under working conditions is crucial to assess salt degradation, the suitability of nanofluids for CSP, and their thermal stability and durability.

This study aims to provide comprehensive insights into the interactions between molten salts-based nanofluids and component materials of the tanks under static working conditions. Specifically, the focus is on the influence of corrosion products on the physical and thermal attributes of silica dioxide nanofluids based on solar salt. The thermal study was conducted at 500 °C for 90 days, following the procedure outlined by Navarro et al. [28]. Four commonly used metal alloys in CSP industry, including AISI 304H, AISI 316 L, AISI 1045, and Inconel 600, were employed in the test, simulating conditions relevant to storage tanks and heat exchanger components. Key properties critical to molten salt implementation in CSP and its reliability over operational cycles, including specific heat capacity, thermal conductivity, viscosity, and chemical composition, were measured. These findings offer a more realistic understanding of nanofluid behaviour under CSP working parameters, facilitating extrapolation for modeling studies throughout a plant's lifespan.

Table 1
Nitrates salt composition in % weight.

KNO_3		$NaNO_3$	
Description	Limits	Description	Limits
Purity	99.7 %	Purity	98 %
Chloride	0.015 %	Chloride	<0.0025 %
Magnesium	0.0005 %	Nitrite	<0.0005 %
Sulphate	0.0005 %	Sulphate	<0.0005 %
Iron	0.0003 %	Carbonate	<0.004 %
Insolubles	0.015 %	Insolubles	<0.0005 %
Moisture	0.04 %	Moisture	<0.2 %

Table 2
AISI 1045, AISI 304H, AISI 316 L and Inconel 600 composition (% wt.).

Metal element (%)	AISI 1045	AISI 304H	AISI 316 L	Inconel 600
Ni	–	7.7	10.27	58.87
Cr	–	19.2	17.23	21.75
Mn	0.75	2.0	1.64	0.21
Mo	–	–	2.2	–
C	0.45	0.08	0.02	0.03
N	–	–	0.1	–
Si	–	0.43	0.52	0.13
P	0.04	–	0.03	–
S	0.05	0.01	0.02	0.1
Al	–	–	–	0.32
Cu	–	–	–	0.03
Fe	Balanced	Balanced	4.12	15.8

The experimental examination of molten salt-based nanofluid properties is contributed to by this paper, with the following objectives: (1) Assess the impact of various corrosion products from four metal alloys on molten salt-based nanofluid properties. (2) Determine the extent to which nanoparticles modify thermophysical and chemical properties following the corrosion test. (3) Provide insights into corrosion mechanisms and the precipitates of corrosion products in nanofluids with metal alloys used as component materials in CSP.

This work presents a novel investigation into the effect of corrosion product precipitates in commercial solar salt-based nanofluids, offering valuable insights that enhance the understanding of nanofluid behaviour. Furthermore, the degradation of solar salt nanofluid properties under operational conditions is explored for the first time. These results contribute significant evidence regarding nanofluid in situ performance, potentially informing innovative strategies to mitigate degradation and corrosion challenges in CSP plants.

2. Materials, methods, and experimental procedures

2.1. Materials

2.1.1. Preparation of molten salts based nanofluids

the molten salts are a commercial binary molten salt mixture (60 % wt. $NaNO_3$ and 40 % wt. KNO_3). Potassium and sodium nitrate, purchased from HAIFA Group and Reagent Chemicals, respectively. Their composition is shown in Table 1. Silica nanoparticles (10–20 nm particle size) were purchased from Sigma Aldrich. As specified by the manufacturer, the shape of the nanoparticles is approximately spherical, and mesoporous form.

The samples formulation started with the preparation of the eutectic mixture through a static melting method, similar to the one reported by Xie et al. [29]. Then, a three-step method, reported by Jo & Banerjee et al. [30], was followed. The raw materials were first dried in an oven at 100 °C for one hour, mixed in the right proportion (60 % wt. $NaNO_3$ and 40 % wt. KNO_3), and heated up to the liquid phase to obtain the eutectic molten salt (300 °C). Nanofluids with 0.5 % wt. and 1 % wt. of

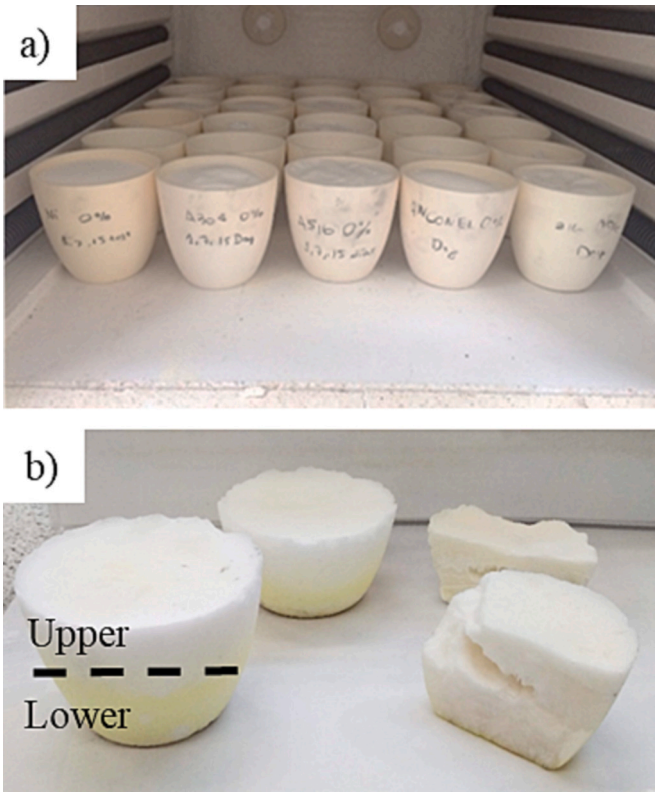

Fig. 1. Solar salt and solar salt-based nanofluids samples; a) samples preparation in crucibles for thermal exposure and, b) samples extracted after the thermal exposure after 90 days, indicating the lower and upper zones of the samples.

nanoparticles concentration were synthesized.

2.1.2. Thermal test

One carbon steel (AISI 1045), two austenitic stainless steel (AISI 316 L, and AISI 304H) and a nickel-chromium alloy (Inconel 600), were chosen to perform the thermal test and analyse the effect on these metals produced on solar salts based on nanofluids composition. These metals are mainly used as material for solar collectors, hot pipes, or the hot salt tank in the two-tank configuration molten salt storage system [31–33]. The metals' composition is detailed in Table 2.

2.2. Experimental procedures

A total immersion of the metals was performed under steady-state conditions in a furnace at 500 °C and an air atmosphere for 90 days, to evaluate the thermos-physical properties of solar salt-based nanofluids under working conditions. The metal alloys samples were a square piece of 10 × 15 and 3 mm of thickness. Each sample was placed inside alumina crucible with the required amount of salt to cover the whole sample surface (around 25 g).

After the thermal exposure, the metal pieces were extracted and the solar salt-based nanofluids samples in contact with the metals were removed from the alumina crucibles and cut into two halves: upper (in contact with the base of the crucible) and lower (in contact with the exterior of the crucible), Fig. 1. Powder samples from both upper and lower parts were taken by grinding them in an Agatha mortar. For a proper samples characterization of the powder samples a standard quartering methodology [34] has been followed to obtain a representative sample, the standard methodology has been adapted for small amount of samples by [35]. The metal samples were subjected to corrosion analysis, the corrosion test was done in [23,28] by the authors.

2.3. Characterization methods

In this section the specifications of the characterization methods are listed; the specific heat capacity, thermal conductivity, and viscosity characterization were performed from [250–500] °C, every 50 °C under the following experimental conditions.

The specific heat capacity, c_p, was determined by Differential Scanning Calorimeter (DSC) using a DSC 3^+ from Mettler Toledo with a constant gas flow of 50 ml/min of N_2. The amount of sample measured was around 24 mg (similar to the sample mass of the sapphire used to calculate the specific heat capacity), an aluminium crucible of 100-μL was used. The areas method was the one selected to measure the specific heat as most has been reported to be the most accurate [36]. For comparison purposes, three different samples were repeated two times (averaged from six values).

The viscosity, υ, was determined by the MCR 502 rheometer from Anton Paar Company with a parallel plate geometry and a 1 mm gap between plates. The tests were performed using the rotational mode with a gap (distance between the sample and the plate) of 1 mm, at a shear rate between 0.1 and 100 s^{-1} under nitrogen atmosphere. The zero-gap, thermal inertia and motor were adjusted and calibrated at the beginning of each test. 24 temperature points were recorded at each temperature step increasing the share rate from 0.1 to 100 s^{-1} following a logarithmic trend. The error of the equipment according to the manufacturer is ±5 %. Note that the samples were repeated three times for comparison purposes.

The thermal conductivity, κ, was calculated from the thermal diffusivity measurements that can be obtained by the temperature rise together with the thickness of the sample according to Eq. (1):

$$\alpha = 0.1388\frac{d^2}{t_{1/2}} \tag{1}$$

where α is the thermal diffusivity (cm^2/s), d is the thickness of the sample (cm), the $t_{1/2}$ is the time at 50 % of the maximum temperature increase (s).

Then the thermal conductivity can be calculated indirectly through a relationship with the specific heat, c_p, and the density, ρ, of the sample using the following Eq. (2):

$$\lambda = \alpha\rho C_p \tag{2}$$

The thermal diffusivity is measured through laser flash, LFA427 from Netzsch, the Rd-Rh platinum crucible is used to contain the sample and the models used to determine the thermal diffusivity is the cowan + corrections. Around 60 mg samples were analysed of 3 mm thickness platinum crucibles and using a 450 V under a gas flow of 100 ml/min of N_2. The bottom and the top of this crucible were coated with a thin graphite layer to enhance the absorption and emission. Two repetitions with a newly prepared crucible fill and three shots for each temperature were performed for each sample.

Inductively Coupled Plasma Atomic Emission Spectroscopy (ICP-AES) and Inductively Coupled Plasma Mass Spectrometry (ICP-MS) was performed to detect and identify the metal elements present in the samples' composition. 100 mg samples were mixed with 1 ml of HNO_3 and 1 ml of HF, for 24 h in an oven at 90 °C. After the 24, 25 ml H_2O (high purity) were added to the mixture. The samples were analysed in two steps; the first step involved using the ICP-AES technique, which was performed on PerkinElmer ELAN 6000 ICP mass spectrometer to analyse Si content and Fe content. In the second step the ICP-MS was employed to analyse Cr, Mn, and Ni-based on the detection limit of the technique, and an ICP-OES simultaneous Perkin Elmer Optima 3200R spectrometer was used to analyse these elements.

3. Results

In this section, the results for the pure solar salts and the molten salt-

Table 3
Thermo-physical properties of pure solar salt and its variations with the incorporation of silica nanoparticles (0.5 % wt. and 1 % wt.).

Temperature (°C)	Nanofluid	Thermal conductivity (W/m·K)	Specific Heat Capacity (J/g·K)	Viscosity (mPa·s)
250	Solar Salt	0.24 ± 0.03	1.28 ± 0.04	11.37 ± 0.45
	Variation (%)			
	0.5 % wt. SiO_2	54	33	105.81
	1 % wt. SiO_2	48	13	129.56
300	Solar Salt	0.26 ± 0.03	1.24 ± 0.05	9.24 ± 1.59
	Variation (%)			
	0.5 % wt. SiO_2	16	1	87.76
	1 % wt. SiO_2	47	9	128.21
350	Solar Salt	0.29 ± 0.04	1.22 ± 0.06	6.78 ± 2.07
	Variation (%)			
	0.5 % wt. SiO_2	33	4	61.85
	1 % wt. SiO_2	59	9	136.24
400	Solar Salt	0.35 ± 0.07	1.27 ± 0.07	5.07 ± 1.2
	Variation (%)			
	0.5 % wt. SiO_2	38	6	2.66
	1 % wt. SiO_2	73	9	100.89
450	Solar Salt	0.45 ± 0.08	1.39 ± 0.07	3.94 ± 0.83
	Variation (%)			
	0.5 % wt. SiO_2	37	4	2.41
	1 % wt. SiO2	43	8	104.70
500	Solar Salt	0.54 ± 0.11	1.57 ± 0.06	2.66 ± 0.17
	Variation (%)			
	0.5 % wt. SiO_2	43	5	37.41
	1 % wt. SiO_2	38	5	188.85

based nanofluids characterization before and after the thermal exposure are described. The effect of nanoparticles concentration and stratification within the samples under study and corrosion products produced during the thermal exposure was analysed in this section.

3.1. Thermo-physical properties of molten salts and molten salt-based nanofluids before thermal exposure

Parameters such as pressure drop, heat exchange, transfer coefficient, heat storage, and tank volume are significantly influenced by the thermophysical properties of Heat Transfer Fluid (HTF) and TES materials. For TES applications, materials with the highest specific heat and high thermal conductivity are imperative to ensure rapid and efficient charging/discharging processes. An increase in specific heat enhances the overall sensible heat storage capacity of TES tanks, while higher thermal conductivity values facilitate improved heat transfer within the TES material by minimizing temperature gradients [37,38]. Moreover, viscosity is a critical factor when considering the use of molten salt as a HTF rather than as a TES medium. This is because a HTF must be pumped through the system's pipes, while a TES medium only requires storage in a tank during the charging/discharging processes. Consequently, viscosity values impact HTF pump operation, pressure drop, and transfer performance [2], ultimately influencing the system's pumping power. As a result, these parameters significantly affect the efficiency and effectiveness of the system. Given that the addition of low concentrations of nanoparticles in ionic systems alters the thermophysical properties of solar salt [19,20,39,40], we shall also compare these properties with those of pure molten salt to comprehend the impact of nanoparticles on property modifications (see Table 3).

As reported in the literature, the addition of nanoparticles has been shown to modify all the examined properties [21,41–44]. In the case of the viscosity, there is an proportional increase with nanoparticles concentration, resulting in up to 144 % enhancement, which aligns with previous findings in the literature [45]. Additionally, temperature exhibits an expected effect on a liquid, with viscosity decreasing as temperature rises [44]. Likewise, both specific heat and thermal conductivity experience greater enhancements with increasing nanoparticles concentration. According to Jiang et al. [40] the addition of 1 % wt. of silica nanoparticles to solar salt demonstrates the best combination of properties for the required operating temperature range in this application (50 °C to 550 °C).

Table 4
Summary of the corrosion products formed during the corrosion test for each salt concentration and time slot [23,28].

Metal	Time Days	Corrosion rate (μm/year) 0 % wt.	0.5 % wt.	1 % wt.	Corrosion product	Corrosion method	Oxides	Interaction with salt
AISI 1045	15	275.70	539.33	552.22	Fe_3O_4, Fe_2O_3	Descaled method	Iron oxides at 15 days. Zinc starts substituting iron to form $ZnFe_2O_4$ at 60 days of the corrosion test. Porous and poor adherence	Localised corrosion, salt permeability through the corrosion products layer
	30	310.47	614.68	720.93	Fe_3O_4, Fe_2O_3			
	60	54.60	394.10	244.86	Fe_3O_4,			
	90	69.81	272.36	313.78	Fe_2O_3, $ZnFe_2O_4$			
AISI 316 L	15	1.84	9.90	14.58	Fe_3O_4, Fe_2O_3	Descaled method	Iron oxides at 15 days. Magnesium starts substituting iron to form MgFeO at 30 days of the corrosion test. Adherence, smooth surface with micro-holes.	Salt permeability into the metal coupon.
	30	5.10	9.14	8.82	Fe_3O_4,			
	60	1.73	5.77	5.94	Fe_2O_3,			
	90	6.60	3.93	4.89	$(Cr, Fe)_2O_4$			
AISI 304H	15	5.14	21.52	19.17	Fe_2O_3	Descaled method	Iron oxides appear at 15 days. Sodium and Chrome start substituting iron to form $NaFeO_2$ and $(Cr, Fe)_2O_4$ at 60 days of the corrosion test Adherence, cracking the surface	Localised corrosion, corrosion oxides precipitated in the intergranular boundary
	30	3.21	12.66	8.88	Fe_2O_3, Fe_3O_4			
	60	6.04	8.55	8.17	Fe_2O_3,			
	90	1.30	6.46	6.25	$Fe3O_4$, $NaFeO_2$, $(Cr,Fe)_2O_4$			
Inconel 600	15	0.68	1.32	1.92	No corrosion product was detected with XRD. The one expected and analysed with EDS is NiO [46,47]	Gravimetric method	No substantial differences can be observed due to the addition of different percentages of nanoparticles Adherence and smooth surface	Low interaction, almost no corrosion was observed
	30	1.66	0.74	1.31				
	60	0.61	0.52	1.29				
	90	0.29	0.11	0.67				

Table 5
ICP of Si, Fe, Mn, Ni, and Cr for the four systems: AISI 304H, Inconel 600, AISI 316 L and AISI 1045 in contact with nanofluids with 0 % wt., 0.5 % wt., and 1 % wt. of nanoparticles (SiO_2) concentration.

Metal	Concentration (% wt.)	Zone	Element's concentration[a]				
			Fe (%)	Mn (%)	Ni (%)	Cr (%)	Si (%)
AISI 304H	1 %	Upper	–	0.00010	–	0.0011	0.02
		Lower	0.009	0.00392	0.00010	0.0139	1.91
	0.5 %	Upper	–	0.00012	–	0.0023	0.04
		Lower	0.002	0.00125	–	0.0059	0.79
	Pure	Upper	–	0.00008	–	–	–
		Lower	–	0.00010	–	0.0020	–
Inconel 600	1 %	Upper	–	0.00006	–	0.0015	0.07
		Lower	0.002	0.00013	0.0002	0.0032	1.32
	0.5 %	Upper	–	0.00008	–	0.0019	0.02
		Lower	0.002	0.00013	0.0002	0.0032	0.21
	Pure	Upper	–	0.00007	–	0.0004	–
		Lower	0.006	0.00018	–	0.0061	–
AISI 316 L	1 %	Upper	–	0.00012	–	0.0008	0.14
		Lower	0.002	0.00028	0.0001	0.0053	1.68
	0.5 %	Upper	–	0.00013	–	0.0014	0.02
		Lower	–	0.00027	–	0.0049	0.42
	Pure	Upper	–	0.00010	–	0.0006	–
		Lower	0.002	0.00016	0.0002	0.0126	–
AISI 1045	1 %	Upper	–	0.00011	–	–	0.07
		Lower	0.011	0.00004	–	–	0.67
	0.5 %	Upper	–	0.00004	–	–	0.02
		Lower	0.027	0.00013	–	–	0.11
	Pure	Upper	–	0.00003	–	–	–
		Lower	0.159	0.00050	–	–	–

[a] Detection limit: 0.002 (Fe), 0.00002 (Mn), 0.0001 (Ni),0.0005 (Cr) and 0.02 (Si).

3.2. Thermo-physical properties of molten salts and molten salt-based nanofluids after thermal exposure

The assessment of nanofluids stability and degradation control is a crucial aspect that must be thoroughly examined to determine their suitability and reliability under real working conditions. This necessitates a comprehensive study encompassing time, temperature, and thermal cycles, especially considering the pronounced corrosion processes molten salts undergo at elevated temperatures. The influence of corrosion products on the properties of solar salt-based nanofluids following a 90-days corrosion test at 500 °C while in contact with various materials such as carbon steel (AISI 1045), two austenitic stainless steels (AISI 316 L and AISI 304H), and a nickel-chromium alloy (Inconel 600) is investigated. It is important to note that corrosion rates for the metal alloys employed in this study have been previously reported by Palacios et al. [23] and Navarro et al. [28]. Table 4 summarizes the results from both of these publications. This paper builds upon the solar salt analysis conducted in the earlier corrosion study, examining its properties and composition. Previous research has indicated that stainless steel alloys strike a balance between corrosion performance and material cost [23], rendering them favourable for implementation in CSP plants. In terms of the nanoparticles' impact, it was concluded that their addition somewhat increases the corrosion rate of alloys exposed to different formulations [28], although this increase could not be directly correlated with nanoparticle content. Data on metal concentration, specific heat capacity, thermal conductivity, and viscosity are presented in this section, linking these factors to provide a more comprehensive understanding of how the attributes and fundamental composition of the salt are affected by corrosion mechanisms.

3.3. Metal concentration

The results obtained by ICP-AES and ICP-MS are presented as a concentration of metal element per unit weight of sample under corresponding to both the upper and lower part of the crucible. The analysis encompassed the determination of the content of iron (Fe), manganese (Mn), nickel (Ni), chromium (Cr), and silicon (Si) elements, as detailed in Table 5, Fig. 2. It is worth nothing that some elements were observed at percentages below the detection limit, as specified in the Table 5. Notably, the Si serves as an indicator of nanoparticles concentration and precipitation rate within the examined sample zone. This provides valuable insights into the preference for nanoparticle deposition within the solar salt following the solidification process.

Chromium and iron are the most prominent elements in the majority of metals, as illustrated in Fig. 2. This aligns well with prior studies on corrosion oxides where hematite, magnetite, and chromium iron oxide were identified as common corrosion products. In the case of AISI 1045, iron emerges as the predominant element. The higher concentration of iron in the lower section of the crucible may be correlated with an increased concentration of nanoparticles in this zone, suggesting which might suggest a favourable disposition of silica with iron oxides. Nevertheless, this hypothesis should be further confirmed through additional tests, such as EDX. Soluble nickel content in the lower section of the samples appears to rise with higher nanoparticles concentration in Inconel 600, AISI 304H and AISI 316 L. As general trend, after 90 days, all dissolved metals exhibit higher concentrations in the lower part of the samples after solidification, which was the expected effect. This phenomenon indicates the low stability and homogeneity of nanoparticles within the solar salt matrix. Conversely, with regard to Fe, Mn, Ni, and Cr concentrations, the samples exhibit contrasting trends:

- Stainless steels: existing literature suggests that after an immersion test, various corrosion products are likely to form due to the interaction between solar salt and stainless steels, such as Fe_3O_4, Fe_2O_3, Cr_2O_3, (Fe, Cr)O_3 in the case of AISI 316 L and Fe_3O_4, Fe_2O_3, (Fe, Cr)$_2O_3$, $NaFeO_2$ for AISI 304H [25,48]. Furthermore, Fe oxides as hematite or magnetite are considered non-protective corrosion products, as demonstrated in the study conducted by Fernández et al. [25]. In contrast, it is suggested by the literature that protective layers can be formed by Ni-Cr-O compounds [25,48].
- Both Mn and Cr elements were detected in the salts and nanofluids for both systems. However, Fe content was only detected in solar salt with 1 % wt. SiO_2 sample in contact with AISI 304H metal alloy. Notably, in the case of AISI 304H, higher nanoparticles content

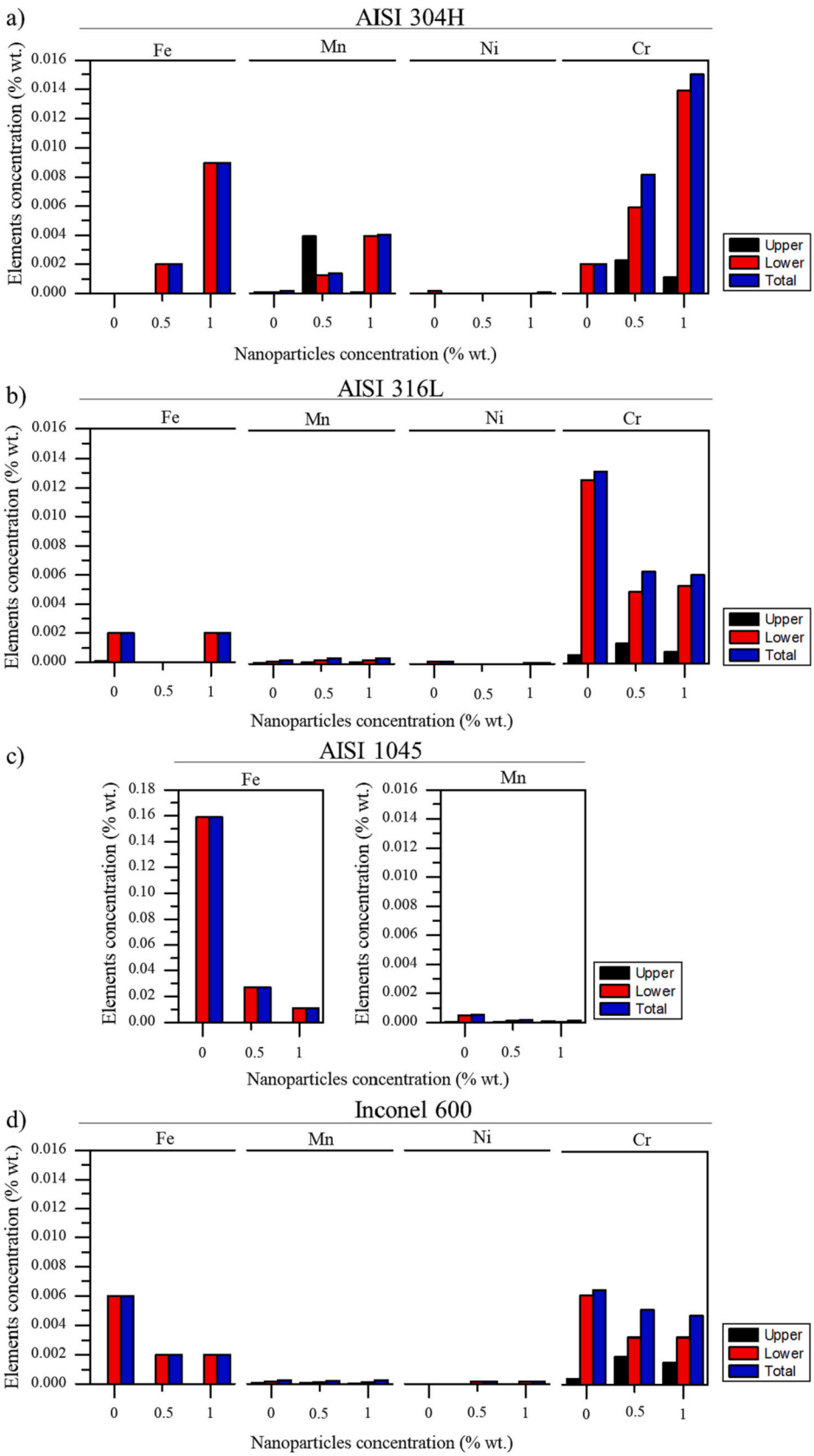

Fig. 2. Elements concentration (Fe, Mn, Ni and Cr) as a function of SiO_2 nanoparticles in the solar salt and solar salt-based nanofluids after 90 days of thermal exposure in the upper and lower part and total in contact with a) AISI 304H, b) AISI 316 L, c) AISI 1045 and, d) Inconel 600.

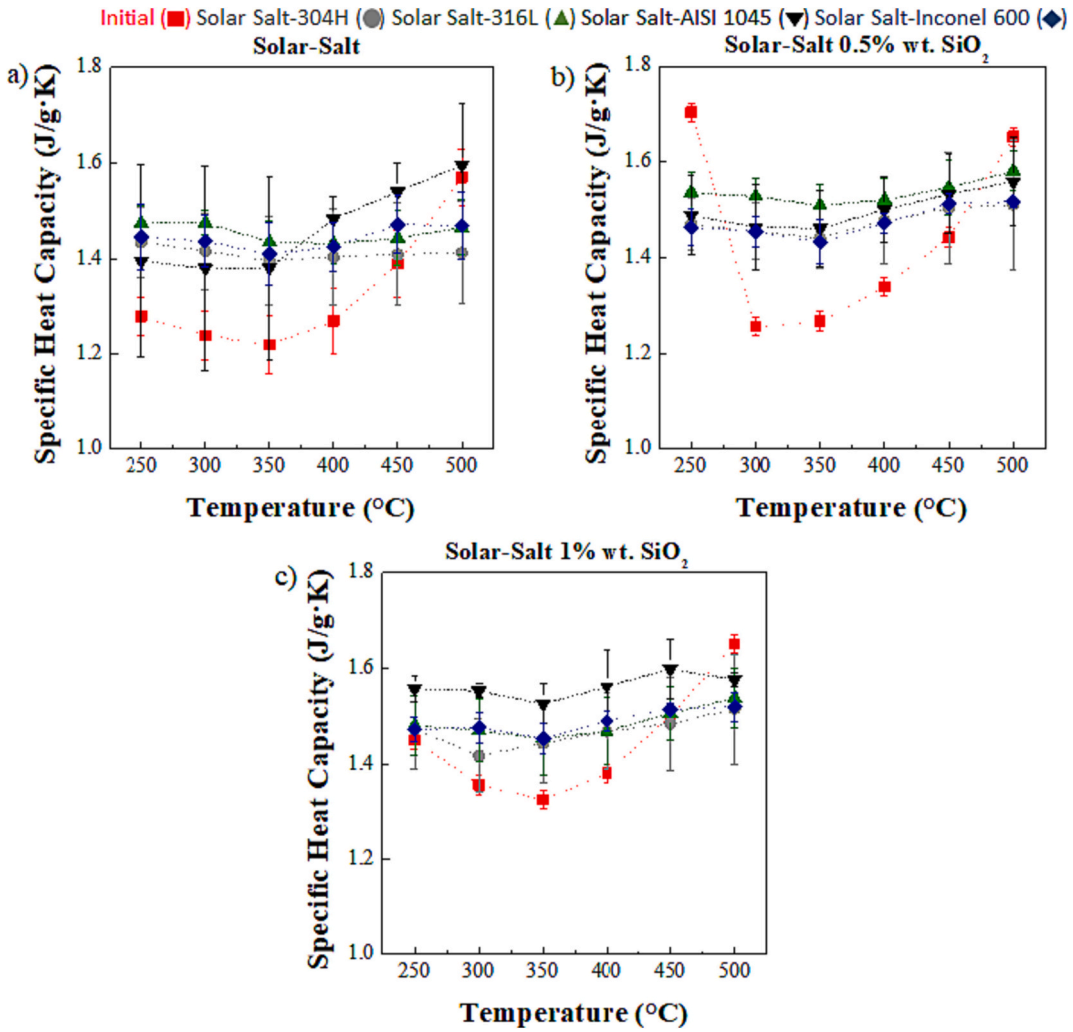

Fig. 3. Specific heat capacity values as a function of the temperature of Solar Salt and nanofluids based Solar Salts, after corrosion test.

corresponds to a greater total concentration of elements. Conversely, for AISI 316 L, both nanofluids exhibit lower concentrations compared to Solar Salt.

- Nickel-chromium alloy: Inconel alloys have been identified as among the alloys exhibiting the lowest mass loss, consequently leading to reduce the corrosion rates. Some of the corrosion products associated with Inconel alloys include $NaFeO_2$, Fe_3O_4, $FeCr_2O_4$, NiO. Moreover, NiO is more protective oxide compared to the iron-based oxides [47]. Based on ICP results, Inconel 600 in contact with solar salt-0.5 % SiO_2 sample shows the lowest concentration of metallic elements. Mn and Cr elements were detected in all the samples under study, demonstrating similar concentrations. In contrast, Fe contents content was exclusively detected in the pure solar salt samples, while Ni content was solely detected in the nanofluids samples.
- Carbon steel: in a study conducted by Navarro et al. [28], it was determined that ZnO is one of the corrosion product. Additionally, the literature reports the formation of various corrosion products like a FeOx components, ZnO and/or $ZnFe_2O_4$ [26,49]. Furthermore, carbon steel is regarded as a less favourable choice due to the low corrosion resistance in contact with molten salts [23]. The presence of both Mn and Fe was detected in all samples in contact with the metallic alloy AISI 1045.

3.3.1. *Specific heat capacity*

Fig. 3 shown the c_p values of Solar Salt (Fig. 3 (a)) and Solar Salt-based nanofluids (Fig. 3 (b) and (c)) after undergoing the thermal exposure within a temperature range of 250 to 500 °C. Given the difficult task of sampling nanofluids with low nanoparticles concentrations and metal elements, and achieving a representative sample [44], the reported values present a significant standard deviation. Nevertheless, discernible trends in the values can be observed in the graphs. The specific heat capacity of the nanofluids after the thermal exposure appear to be higher, attributed to the presence of metal elements within the salt. This observation is consistent with findings in the literature, which have also reported elevated values after corrosion test [46]. Consequently, the stored sensible heat in the storage tanks will not be affected negatively by solar salts degradation. In the case of solar salt 0.5 % wt. SiO_2 system (Fig. 3 (b)), the samples in contact with AISI 316 L, shows improved thermal performance, with enhancements regarding between 20 and 25 %, in the temperature range from 300 °C to 450 °C. Nonetheless, statistically significant differences were not observed between the samples exposed to the four metal alloys. Furthermore, in the solar salt-1 % wt. NP system (Fig. 3 (c)), the sample in contact with the carbon steel has the greatest c_p. The differences between the rests of the samples were statistically non-significant. Moreover, for samples in contact with Inconel 600, AISI 304H and AISI 316 L, the c_p falls below values at temperatures up to 350 °C. Conversely, between 350 °C and approximately 500 °C, c_p increases with temperature, with Inconel 600 showing a 40 % increase and 24 % in the case of the AISI 1045. After the thermal exposure, the solar salt-0.5 % SiO_2-AISI 316 L and solar salt-1 % SiO_2-AISI 1045 systems exhibit the most favourable thermal

Table 6
Enthalpy of fusion (ΔH_m) and melting temperatures (T_{onset}, T_{peak} and T_{endset}) of Solar Salt and Solar Salt-based nanofluids after corrosion test, taking as reference pure Solar Salt without metal alloys contact.

Sample	ΔHm	T onset	T peak	T endset
	± 0.1 J/g	± 0.1 °C	± 0.1 °C	± 0.1 °C
REF (Pure Solar Salt)	**−109.0**	**225.7**	**224.7**	**227.8**
Pure Solar Salt – AISI 304H	−134.5	207.6	213.6	233.9
Solar Salt - 0.5 % SiO_2 - AISI 304H	−130.3	208.9	215.9	227.1
Solar Salt - 1 % SiO_2 - AISI 304H	−142.1	208.4	215.8	236.0
Pure Solar Salt – AISI 316 L	−141.0	206.7	216.9	231.1
Solar Salt - 0.5 % SiO_2 - AISI 316 L	−129.0	216.1	217.0	238.1
Solar Salt - 1 % SiO2 - AISI 316 L	−128.5	204.3	211.7	233.8
Pure Solar Salt - AISI 1045	−136.6	201.1	212.3	263.2
Solar Salt - 0.5 % SiO_2 - AISI 1045	−128.6	203.2	211.3	222.8
Solar Salt - 1 % SiO_2 - AISI 1045	−133.6	204.7	212.9	214.2
Pure Solar Salt - Inconel 600	−135.6	207.3	214.3	229.9
Solar Salt - 0.5 % SiO_2 - Inconel 600	−137.7	208.5	216.3	230.1
Solar Salt - 1 % SiO_2 - Inconel 600	−131.3	207.2	213.1	225.1

performance.

The parameters of melting enthalpy and melting temperatures (T_{onset}, T_{peak} and, T_{end}) for all the samples following the thermal exposure are summarized in Table 6. The pure solar salt, subjected to the same heat treatment without any metallic contact has been taken as a reference. All samples subjected to the thermal exposure had a higher melting enthalpy compared to the reference, with enhancements of up to 30 %. Among these, the solar salt-1 % SiO_2–AISI 304H samples displayed the highest enthalpy of fusion. Conversely, both T_{onset} (the temperature at the melting process starts) and T_{peak} demonstrated a decrease of up to 11 % and 6 % when compared to the reference, respectively. Instead, no specific correlation was observed in the behaviour of the T_{end} (the temperature at which the sample is completely melted). The reduction in melting temperature reduces the operational temperature of the cold storage tank, thereby preventing corrosion risks and solidification of the molten salts.

As reported by [46], the broadening of the melting point is a consequence of the non-eutectic properties of the mixture. Each constituent within the mixture exhibits a distinct melting temperature, contributing to a broader melting range. These variations in melting points strongly suggest that metal impurities resulting from corrosion are likely factors behind alterations in the melting point of the salts mixture. Investigating the correlation between nitrite concentration and the melting point is essential for elucidating the connection between them. Furthermore, exploring correlations between other impurities and the melting point should also be considered in order to establish their relationships.

3.3.2. *Thermal conductivity*

The thermal conductivity values after the thermal exposure of Solar Salt-based nanofluids, within the temperature range of 250 to 500 °C, are presented in Fig. 4. Solar Salt, Fig. 4 (a), and Solar Salt-based nanofluids, Fig. 4 (b) and (c), a similar behaviour is observed in comparison to the base thermal conductivity. In the pure Solar Salt samples, Fig. 4 (a), two distinct temperature regimes can be identified. The first spans from 250 °C and 350 °C, where thermal conductivity remains practically constant for all samples. The second regime, spanning from 350 °C to 500 °C, demonstrates improved thermal conductivity, which

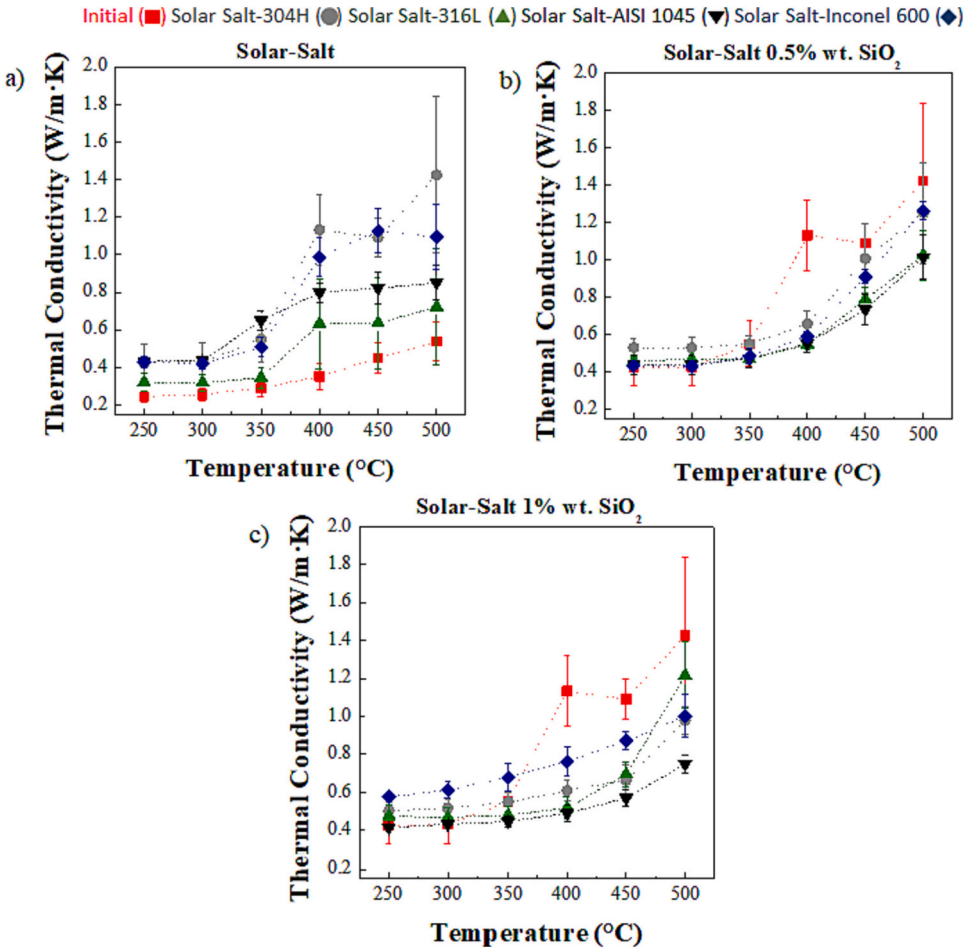

Fig. 4. Thermal conductivity values as a function of the temperature of Solar Salt and nanofluids based Solar Salt, after corrosion test.

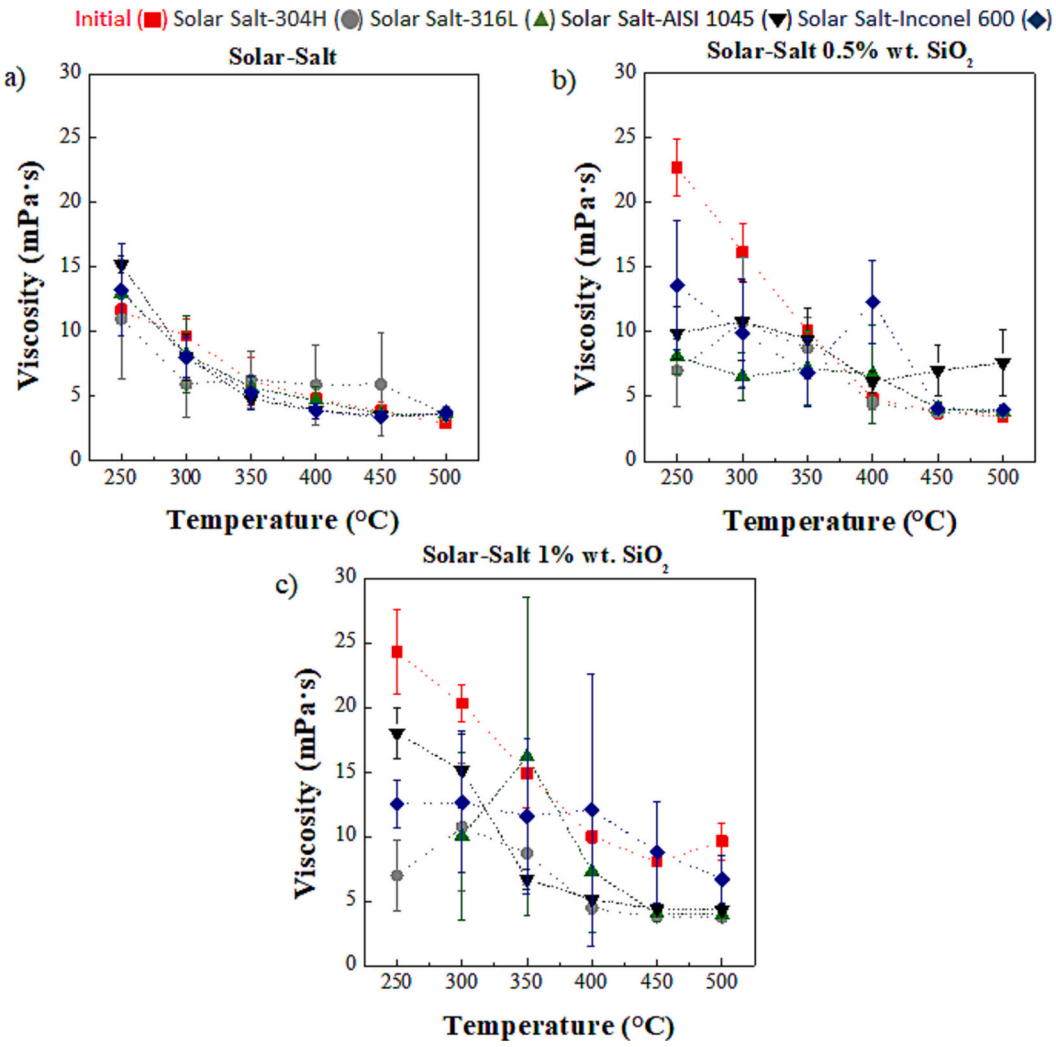

Fig. 5. Viscosity values as a function of temperature for Solar Salt and Solar Salt based nanofluids, after corrosion test.

remains constant within this temperature range. Additionally, sample in contact with Inconel 600, AISI 304H and AISI 1045 exhibit statistically higher thermal conductivity than those in contact with AISI 316 L. However, all samples shown enhanced thermal conductivity compared to the initial sample before the thermal exposure, except for AISI 316 L, which shows an opposite trend. Conversely, nanofluids exhibit a different behaviour. In the case of the Solar Salt- 0.5 % wt. system, Fig. 4 (b) no statistical significant differences were observed among all samples from 250 °C to 350 °C. At 400 °C, all samples subjected to the thermal exposure have lower thermal conductivity than the initial sample. Finally, from 450 to 500 °C, the deviation between the initial sample and post-thermal exposure was lower. A similar trend is observed in the Solar Salt-1 % wt. system, Fig. 4 (c), except for the nanofluid in contact with Inconel 600, which exhibits higher thermal conductivity than the initial sample within the temperature range of 250 °C to 350 °C. Despite TES systems typically operating above the 300–400 °C temperature range, the Solar Salt-1 % SiO_2 - Inconel-600 system demonstrated the highest thermal conductivity values after the thermal exposure, ranging between 0.6 and 0.8 $W{\cdot}m^{-1}{\cdot}K^{-1}$. Consequently, no significant modifications are observed for the rest of the nanofluids samples within this temperature range.

3.3.3. *Rheology*

In addition to c_p and thermal conductivity, viscosity represents a crucial parameter in thermal applications, especially when utilized as a HTF. The convective heat transfer coefficient is notably influenced by viscosity. Moreover, fluids with a higher viscosity than the base fluid result in an increase in pressure drop and consequently an increase in the power required for pumping [45]. Viscosity in nanofluids primarily increases with rising nanoparticles concentration and decreases by increasing the temperature. The viscosity values after the corrosion test of Solar Salt-based nanofluids, in the temperature range from 250 to 500 °C, were presented in Fig. 5. Three remarkable features can be extracted. First, there is a noticeable lack of uniformity and high standard deviation in the samples post-thermal exposure, particularly evident in the nanofluids samples. These scattered results can be attributed to the presence of particles and nanoparticles, which significantly influence fluid behaviour. Second, nanoparticles contribute to increased viscosity, but their effect diminishes after the thermal exposure, resulting in either similar or lower values compared to samples without nanoparticles. This suggests that the effect of nanoparticles on viscosity is not a constant over time. Third, the viscosity of nanofluid samples tends to decrease after the thermal exposure when compared to the initial samples. In the case of the Solar Salt system, Fig. 5 (a), no significant changes are observed in any sample after the test. It is worth noting the considerable standard deviation in the Solar Salt sample in contact with AISI 304H compared to the other samples. For the Solar Salt- 0.5 % wt. system, Fig. 5 (b), the sample in contact with AISI 316 L shows better temperature stability within the range of 250 °C to 350 °C. Lastly, the Solar Salt-1 % wt. system, Fig. 5 (c), concerning average

values, the sample in contact with Inconel 600 demonstrates better temperature stability, despite the high standard deviation. Consequently, the incorporation of nanoparticles impacts the rheological behaviour by increasing the pressure drop within and subsequently reducing it over time.

4. Conclusions

A thermal exposure at 500 °C for 3 months (2160 h) was carried out. The test involved Solar Salt samples and two formulated Solar Salt-based nanofluids containing 0.5 % and 1 % wt. of SiO_2 nanoparticles. These were placed in contact with various metals, including carbon steel (AISI 1045), two stainless steels (AISI 304H and AISI 316 L) and Nickel-chromium alloy (Inconel 600). This study represents the first comprehensive analysis of the effect of corrosion products and temperature-time on the thermo-physical properties, both before and after the thermal exposure. The following conclusions can be drawn from the characterization:

- Corrosion products were identified in the samples after the thermal exposure: (1) Nanofluids in contact with AISI 316 L stainless steel exhibited a lower concentration of corrosion products compared to AISI 304H steel. (2) The Fe content in Inconel 600 and AISI 1045 samples decreased in nanofluids. (3) Among the samples in contact with Inconel 600 and AISI 1045, the formed displayed the lowest concentration of corrosion products, while the latter exhibited the highest.
- The thermophysical properties of Solar Salt and nanofluids after the thermal exposure have been altered. Specific heat capacity values improved for all samples in contact with metal alloys, with nanofluids showing greater thermal stability and lower dispersion compared to Solar Salt samples. Thermal conductivity values in nanofluids exhibited smaller modifications compared to the initial samples when compared to Solar Salt. Consequently, nanofluid demonstrate greater stability over time concerning thermal conductivity. Notably, the presence of corrosion products had the most significant impact on viscosity values post-thermal exposure. The influence of nanoparticles diminished over time, with nanofluids samples eventually exhibiting values similar to Solar Salt, but with higher deviations.
- Nanofluids were presented as suitable fluids for TES applications, boasting improved thermo-physical properties. Importantly, these properties did not worsened following the thermal exposure.

This study was demonstrated the low modification of molten salt properties under service conditions. As well, the presence of nanoparticles in molten salts contributed to a reduction in the percentage of corrosion products, thus aiding in the reduction of the corrosion rate.

In conclusion, this study provides reliable data of the key thermo-physical properties in-service and its compatibility with AISI 1045, AISI 304H, AISI 316 L and Inconel 600 metal alloys, facilitating the design of more accurate TES systems with a more realistic approach to their efficiency and effectiveness.

CRediT authorship contribution statement

Adela Svobodova-Sedlackova: Data curation, Formal analysis, Investigation, Visualization, Writing – original draft. **Anabel Palacios:** Data curation, Formal analysis, Visualization, Writing – original draft. **Zhu Jiang:** Data curation. **A. Ines Fernández Renna:** Conceptualization, Funding acquisition. **Yulong Ding:** Conceptualization, Funding acquisition. **Helena Navarro:** Conceptualization, Formal analysis, Methodology, Supervision, Writing – review & editing. **Camila Barreneche:** Conceptualization, Methodology, Supervision, Writing – review & editing.

Declaration of competing interest

The authors declare that they have no known competing financial interests or personal relationships that could have appeared to influence the work reported in this paper.

Data availability

Data will be made available on request.

Acknowledgements

This work was partially funded by the Ministerio de Economía y Competitividad de España RTI2018-093849-B-C32 and PID2021-123511OB-C32 MCIN/AEI/10.13039/501100011033. The authors would like to thank the Catalan Government for the quality accreditation given to their research group (DIOPMA 2021 SGR 00708). DIOPMA is a certified agent TECNIO in the category of technology developers from the Government of Catalonia. This work is a contribution to the COST (European Cooperation in Science and Technology) Action CA15119: Overcoming Barriers to Nanofluids Market Uptake (NANOUPTAKE). This work is partially supported by 100 Foreign Experts Plan of Hebei Province.

References

[1] International Energy Agency. www.iea.org, 2020.
[2] G. Peiró, J. Gasia, L. Miró, C. Prieto, L.F. Cabeza, Influence of the heat transfer fluid in a CSP plant molten salts charging process, Renew. Energy 113 (2017) 148–158, https://doi.org/10.1016/j.renene.2017.05.083.
[3] G. Peiró, C. Prieto, J. Gasia, A. Jové, L. Miró, L.F. Cabeza, Two-tank molten salts thermal energy storage system for solar power plants at pilot plant scale: lessons learnt and recommendations for its design, start-up and operation, Renew. Energy 121 (2018) 236–248, https://doi.org/10.1016/j.renene.2018.01.026.
[4] S.S. Mostafavi Tehrani, R.A. Taylor, K. Nithyanandam, A. Shafiei Ghazani, Annual comparative performance and cost analysis of high temperature, sensible thermal energy storage systems integrated with a concentrated solar power plant, Sol. Energy 153 (2017) 153–172, https://doi.org/10.1016/j.solener.2017.05.044.
[5] S. Torras, C.D. Pérez-segarra, I. Rodríguez, J. Rigola, A. Oliva, Parametric study of two-tank TES systems for CSP plants, Energy Procedia 69 (2015) 1049–1058, https://doi.org/10.1016/j.egypro.2015.03.206.
[6] S. Guillot, A. Faik, A. Rakhmatullin, J. Lambert, E. Veron, P. Echegut, C. Bessada, N. Calvet, X. Py, Corrosion effects between molten salts and thermal storage material for concentrated solar power plants, Appl. Energy 94 (2012) 174–181, https://doi.org/10.1016/j.apenergy.2011.12.057.
[7] U. Pelay, L. Luo, Y. Fan, D. Stitou, M. Rood, Thermal energy storage systems for concentrated solar power plants, Renew. Sustain. Energy Rev. 79 (2017) 82–100, https://doi.org/10.1016/j.rser.2017.03.139.
[8] A. Palacios, C. Barreneche, M.E. Navarro, Y. Ding, Thermal energy storage technologies for concentrated solar power – a review from a materials perspective, Renew. Energy 156 (2020) 1244–1265, https://doi.org/10.1016/j.renene.2019.10.127.
[9] C. Prieto, R. Osuna, A.I. Fernández, L.F. Cabeza, Thermal storage in a MW scale. Molten salt solar thermal pilot facility: plant description and commissioning experiences, Renew. Energy 99 (2016) 852–866, https://doi.org/10.1016/j.renene.2016.07.053.
[10] C. Prieto, R. Osuna, A.I. Fernández, L.F. Cabeza, Thermal storage in a MW scale. Molten salt solar thermal pilot facility: plant description and commissioning experiences, Renew. Energy 99 (2016) 852–866, https://doi.org/10.1016/j.renene.2016.07.053.
[11] G. Alva, Y. Lin, G. Fang, An overview of thermal energy storage systems, Energy 144 (2018) 341–378, https://doi.org/10.1016/j.energy.2017.12.037.
[12] Y. Grosu, U. Nithiyanantham, A. Zaki, A. Faik, A simple method for the inhibition of the corrosion of carbon steel by molten nitrate salt for thermal storage in concentrating solar power applications, Npj Mater. Degrad. 2 (2018) 1–8, https://doi.org/10.1038/s41529-018-0055-0.
[13] H. Tiznobaik, D. Shin, Enhanced specific heat capacity of high-temperature molten salt-based nanofluids, Int. J. Heat Mass Transf. 57 (2013) 542–548, https://doi.org/10.1016/j.ijheatmasstransfer.2012.10.062.
[14] A. Alirezaie, M.H. Hajmohammad, A. Alipour, Do nanofluids affect the future of heat transfer?"A benchmark study on the efficiency of nanofluids&quot, Energy 157 (2018), https://doi.org/10.1016/J.ENERGY.2018.05.060.
[15] A. Wahab, A. Hassan, M. Arslan, H. Babar, M. Usman, Solar energy systems – potential of nanofluids, J. Mol. Liq. 289 (2019), https://doi.org/10.1016/j.molliq.2019.111049.
[16] K. Khanafer, K. Vafai, A review on the applications of nanofluids in solar energy field, Renew. Energy 123 (2018) 398–406, https://doi.org/10.1016/j.renene.2018.01.097.

[17] S. Akilu, K.V. Sharma, A. Tesfamichael, R. Mamat, A review of thermophysical properties of water based composite nano fl uids, Renew. Sustain. Energy Rev. (2016), https://doi.org/10.1016/j.rser.2016.08.036.
[18] S.A. Angayarkanni, J. Philip, Review on thermal properties of nanofluids: recent developments, Adv. Colloid Interface Sci. 225 (2015) 146–176, https://doi.org/10.1016/j.cis.2015.08.014.
[19] A. Svobodova-Sedlackova, C. Barreneche, G. Alonso, A.I. Fernandez, P. Gamallo, Effect of nanoparticles in molten salts – MD simulations and experimental study, Renew. Energy 152 (2020) 208–216, https://doi.org/10.1016/j.renene.2020.01.046.
[20] X. Wei, Y. Yin, B. Qin, W. Wang, J. Ding, J. Lu, Preparation and enhanced thermal conductivity of molten salt nanofluids with nearly unaltered viscosity, Renew. Energy 145 (2020) 2435–2444, https://doi.org/10.1016/j.renene.2019.04.153.
[21] W. Wang, Z. Wu, B. Li, B. Sundén, A review on molten-salt-based and ionic-liquid-based nanofluids for medium-to-high temperature heat transfer, J. Therm. Anal. Calorim. 136 (2019) 1037–1051, https://doi.org/10.1007/s10973-018-7765-y.
[22] R. Bubbico, G.P. Celata, F. D'Annibale, B. Mazzarotta, C. Menale, Experimental analysis of corrosion and erosion phenomena on metal surfaces by nanofluids, Chem. Eng. Res. Des. 104 (2015) 605–614, https://doi.org/10.1016/j.cherd.2015.10.004.
[23] A. Palacios, M.E. Navarro, Z. Jiang, A. Avila, G. Qiao, E. Mura, Y. Ding, High-temperature corrosion behaviour of metal alloys in commercial molten salts, Sol. Energy 201 (2020) 437–452, https://doi.org/10.1016/j.solener.2020.03.010.
[24] B. Ma, D. Shin, D. Banerjee, One-step synthesis of molten salt nanofluid for thermal energy storage application – a comprehensive analysis on thermophysical property, corrosion behavior, and economic benefit, J. Energy Storage 35 (2021), 102278, https://doi.org/10.1016/j.est.2021.102278.
[25] A.G. Fernández, B. Muñoz-Sánchez, J. Nieto-Maestre, A. García-Romero, High temperature corrosion behavior on molten nitrate salt-based nanofluids for CSP plants, Renew. Energy 130 (2019) 902–909, https://doi.org/10.1016/j.renene.2018.07.018.
[26] U. Nithiyanantham, Y. Grosu, A. Anagnostopoulos, E. Carbó-Argibay, O. Bondarchuk, L. González-Fernández, A. Zaki, J.M. Igartua, M.E. Navarro, Y. Ding, A. Faik, Nanoparticles as a high-temperature anticorrosion additive to molten nitrate salts for concentrated solar power, Sol. Energy Mater. Sol. Cells. 203 (2019), 110171, https://doi.org/10.1016/j.solmat.2019.110171.
[27] U. Nithiyanantham, Y. Grosu, L. González-Fernández, A. Zaki, J.M. Igartua, A. Faik, Corrosion aspects of molten nitrate salt-based nanofluids for thermal energy storage applications, Sol. Energy 189 (2019) 219–227, https://doi.org/10.1016/j.solener.2019.07.050.
[28] M.E. Navarro, A. Palacios, Z. Jiang, A. Avila, G. Qiao, E. Mura, Y. Ding, Effect of SiO2 nanoparticles concentration on the corrosion behaviour of solar salt-based nanofluids for concentrating solar power plants, Sol. Energy Mater. 247 (2022), 111923.
[29] Q. Xie, Q. Zhu, Y. Li, Thermal storage properties of molten nitrate salt-based nanofluids with graphene nanoplatelets, Nanoscale Res. Lett. 11 (2016) 306, https://doi.org/10.1186/s11671-016-1519-1.
[30] B. Jo, D. Banerjee, Enhanced specific heat capacity of molten salt-based nanomaterials: effects of nanoparticle dispersion and solvent material, Acta Mater. 75 (2014) 80–91, https://doi.org/10.1016/j.actamat.2014.05.005.
[31] M. Jonemann, Advanced Thermal Storage System with Novel Molten Salt, Subcontract Rep. - NREL/SR-5200-58595. http://www.nrel.gov/docs/fy13osti/58595.pdf, 2013.
[32] Y. Mori, High Temperature Heat Exchangers, Heat Transf. Proc. Int. Heat Transf. Conf. 1 (1986) 259–268, https://doi.org/10.1115/1.3264915.
[33] R. Moore, M. Vernon, C.K. Ho, N.P. Siegel, G.J. Kolb, S.N. Laboratories, P.O. B. Albuquerque, Design considerations for concentrating solar power tower systems employing molten salt, Security 1–51 (2010).
[34] Standard practice for reducing samples of aggregate to testing size 1, Astm C 702–9 (04) (2003) 700–703.
[35] A. Svobodova-sedlackova, C. Barreneche, P. Gamallo, A.I. Fernández, Specific Heat Capacity of nanofluids: A Sampling Study 32, 2021, p. 120682.
[36] G. Ferrer, C. Barreneche, A. Solé, I. Martorell, L.F. Cabeza, New proposed methodology for specific heat capacity determination of materials for thermal energy storage (TES) by DSC, J. Energy Storage 11 (2017) 1–6, https://doi.org/10.1016/j.est.2017.02.002.
[37] J. Gasia, L. Miró, L.F. Cabeza, Review on system and materials requirements for high temperature thermal energy storage. Part 1: general requirements, Renew. Sustain. Energy Rev. 75 (2017) 1320–1338, https://doi.org/10.1016/j.rser.2016.11.119.
[38] M.S. Bretado-De los Rios, C.I. Rivera-Solorio, K.D.P. Nigam, An overview of sustainability of heat exchangers and solar thermal applications with nanofluids: a review, renew, Sustain. Energy Rev. 142 (2021), 110855, https://doi.org/10.1016/j.rser.2021.110855.
[39] A.R. Prasad, S. Singh, H. Nagar, A review on nanofluids: properties and applications, Int. J. Adv. Res. Innov. Ideas Educ. 3 (2017) 3185–3209.
[40] Z. Jiang, A. Palacios, X. Lei, M.E. Navarro, G. Qiao, E. Mura, Novel key parameter for eutectic nitrates based nanofluids selection for concentrating solar power (CSP) systems, Appl. Energy 235 (2019) 529–542, https://doi.org/10.1016/j.apenergy.2018.10.114.
[41] G. Yıldız, Ü. Ağbulut, A.E. Gürel, A review of stability, thermophysical properties and impact of using nanofluids on the performance of refrigeration systems, Int. J. Refrig. 129 (2021) 342–364, https://doi.org/10.1016/j.ijrefrig.2021.05.016.
[42] M. Awais, A.A. Bhuiyan, S. Salehin, M.M. Ehsan, B. Khan, M.H. Rahman, Synthesis, heat transport mechanisms and thermophysical properties of nanofluids: a critical overview, Int. J. Thermofluids. 10 (2021), 100086, https://doi.org/10.1016/j.ijft.2021.100086.
[43] N. Sezer, M.A. Atieh, M. Koç, A comprehensive review on synthesis, stability, thermophysical properties, and characterization of nanofluids, Powder Technol. 344 (2019) 404–431, https://doi.org/10.1016/j.powtec.2018.12.016.
[44] K. Bashirnezhad, S. Bazri, M.R. Safaei, M. Goodarzi, M. Dahari, O. Mahian, A. S. Dalkiliça, S. Wongwises, Viscosity of nanofluids: a review of recent experimental studies, Int. Commun. Heat Mass Transf. 73 (2016) 114–123, https://doi.org/10.1016/j.icheatmasstransfer.2016.02.005.
[45] A. Kumar, S. Subudhi, Preparation, characterization and heat transfer analysis of nano fl uids used for engine cooling, Appl. Therm. Eng. 160 (2019), 114092, https://doi.org/10.1016/j.applthermaleng.2019.114092.
[46] A.M. Kruizenga, D.D. Gill, M. Laford, G. Mcconohy, Corrosion of High Temperature Alloys in Solar Salt at 400, 500, and 680 ° C, Sandia Rep. (2013) 1–45.
[47] G. McConohy, A. Kruizenga, Molten nitrate salts at 600 and 680°C: Thermophysical property changes and corrosion of high-temperature nickel alloys, Sol. Energy 103 (2014) 242–252, https://doi.org/10.1016/j.solener.2014.01.028.
[48] D.H. Abdeen, M.A. Atieh, B. Merzougui, W. Khalfaoui, Corrosion evaluation of 316L stainless steel in CNT-water nanofluid: effect of CNTs loading, Materials (Basel) 12 (2019), https://doi.org/10.3390/ma12101634.
[49] F.J. Ruiz-Cabañas, C. Prieto, R. Osuna, V. Madina, A.I. Fernández, L.F. Cabeza, Corrosion testing device for in-situ corrosion characterization in operational molten salts storage tanks: A516 Gr70 carbon steel performance under molten salts exposure, Sol. Energy Mater. Sol. Cells 157 (2016) 383–392, https://doi.org/10.1016/j.solmat.2016.06.005.